Overexpression of Rhodopsin Alters the Structure and Photoresponse of Rod Photoreceptors

Xiao-Hong Wen,[†*] Lixin Shen,[‡] Richard S. Brush,[§] Norman Michaud,[†] Muayyad R. Al-Ubaidi,[§] Vsevolod V. Gurevich,[‡] Heidi E. Hamm,[‡] Janis Lem,[¶] Emmanuele DiBenedetto,[‖] Robert E. Anderson,[§] and Clint L. Makino[†]

[†]Department of Ophthalmology, Massachusetts Eye and Ear Infirmary and Harvard Medical School, Boston, Massachusetts; [‡]Department of Pharmacology, Vanderbilt University Medical Center, Nashville, Tennessee; [§]Departments of Cell Biology and Ophthalmology, University of Oklahoma Health Science Center, Oklahoma City, Oklahoma; [¶]Department of Ophthalmology, Program in Genetics, Program in Neuroscience, and Program in Cell, Molecular and Developmental Biology, Tufts University School of Medicine, Boston, Massachusetts; and [‖]Department of Mathematics, Vanderbilt University, Nashville, Tennessee

ABSTRACT Rhodopsins are densely packed in rod outer-segment membranes to maximize photon absorption, but this arrangement interferes with transducin activation by restricting the mobility of both proteins. We attempted to explore this phenomenon in transgenic mice that overexpressed rhodopsin in their rods. Photon capture was improved, and, for a given number of photoisomerizations, bright-flash responses rose more gradually with a reduction in amplification—but not because rhodopsins were more tightly packed in the membrane. Instead, rods increased their outer-segment diameters, accommodating the extra rhodopsins without changing the rhodopsin packing density. Because the expression of other phototransduction proteins did not increase, transducin and its effector phosphodiesterase were distributed over a larger surface area. That feature, as well as an increase in cytosolic volume, was responsible for delaying the onset of the photoresponse and for attenuating its amplification.

INTRODUCTION

G-protein-coupled receptors appeared early in the evolutionary development of plant and animal species, and these receptors remain in most species for the detection of many different extracellular substances (1–3); ~800 genes encode for G-protein-coupled receptors in humans. Sensitivity of detection depends on the number of receptors expressed on the membrane and the amplification of the signal transduction pathway. In retinal rods, in which high sensitivity and quick response are equally important for survival, the level of rhodopsin expression on the membrane surface can conflict with amplification and rapid-response kinetics. To minimize the conflict, variability in the photon capture of rods usually arises from differences in the number of rhodopsin-bearing membrane layers, rather than from differences in the packing density of rhodopsin in the outer-segment membranes. The latter mechanism appears to be reserved for extreme conditions, such as in the rearing of albino rats under very bright light (4,5). The close apposition of many membrane layers may require a certain minimal density of rhodopsins to help maintain the separation of the layers, because decreasing rhodopsin expression results in rod cell degeneration or failure to form an outer segment (6,7). In addition, maintenance of rhodopsin packing density below a certain maximum may be necessary to avoid an adverse impact downstream in the transduction cascade.

In the first amplifying step of phototransduction, photoexcited rhodopsins sequentially collide with and activate many transducin G-protein molecules (8,9). Transducin activates a phosphodiesterase (PDE) that hydrolyzes cyclic guanosine monophosphate (cGMP). The resultant fall in intracellular cGMP closes cyclic nucleotide gated (CNG) cation channels in the plasma membrane. A high density of rhodopsin in the membrane promotes efficient photon capture, but, after a photon is absorbed, the neighboring, catalytically inactive, rhodopsins could block access of the photoexcited rhodopsins to transducins (10). A critical density may even induce rhodopsin to oligomerize (11–13). Thus, upon hemizygous knockout of rhodopsin to remove half of the rhodopsins from the membrane, photoexcited rhodopsins activate transducins at a faster rate, accelerating the rising phase of the photoresponse (14). (See Liang et al. (15) for an alternative interpretation.) On the other hand, an overly crowded membrane would slow the photoresponse and could potentially block it completely. To find out whether rod photoreceptors approach that point, photoresponses were recorded from rods of mice that carried a transgene for rod opsin to bolster rhodopsin expression.

METHODS

Transgenic mice

Fertilized embryos from line A of the Bouse-expressing mouse colony (16) at the University of Oklahoma Health Sciences Center were implanted into foster mothers at the New England Eye Center. The expressed Bouse transgene was a modified mouse genomic rod opsin with three carboxy terminal substitutions that confer immunogenicity to bovine opsin antibody. Presence of the transgene was analyzed using a polymerase chain reaction (PCR) strategy adapted from Tan et al. (16): MRA225 (sense), 5′AAA GCA

Submitted April 18, 2008, and accepted for publication October 8, 2008.

*Correspondence: wenx@meei.harvard.edu

Editor: Janos K. Lanyi.

0006-3495/09/02/0939/12 $2.00

doi: 10.1016/j.bpj.2008.10.016

GGC TGT GAA GCA CAC TGC and MRA226 (antisense), 5′ GTC TTG GAA ACG GTG GTA GAG GCC. In addition, a third primer was designed to provide an internal control for endogenous mouse opsin: Bouse R (antisense), 5′ TCC ATG TGT CCT GTG GAT GCG TAG. Annealing temperature was ramped from 80 to 74°C, with extension at 72°C. The endogenous opsin yielded a 526-basepair PCR product, whereas the Bouse transgene yielded a 669-basepair PCR product. Offspring from the foster mothers were used in all subsequent breedings. Bouse+/− mice were crossed with homozygous rhodopsin knockout (R−/−) mice (7) to generate both Bouse+/−, R+/− and Bouse+/−, R−/− mice. Homozygous Bouse (+/+) mice were also produced. Bouse+/+ could not be distinguished from Bouse+/− by PCR. Therefore, mice in question were bred with wild-type (WT), and their progeny were analyzed; all offspring from matings with a Bouse+/+ were Bouse positive. One difference between the New England Eye Center mice colony and the mice colony studied at Oklahoma was that, in the former, crossings were with B6D2F1, whereas, in the latter, FVB/NxC57BL/6 hybrids were used.

The original intent was to systematically vary rhodopsin expression in transgenic mouse rods so that changes in flash response sensitivity and kinetics could be quantified over a wide range of rhodopsin packing densities in the membrane. However, mice expressing Bouse on either an R−/− or an R+/− genetic background sustained widespread photoreceptor degeneration at an early age (not shown). Backcrosses on an R−/− genetic background may have resulted in mice that produced too little rhodopsin for rod viability (6,7,17), but a lethal deficiency was not expected from crosses of Bouse+/− with R+/−. Bouse+/+ also demonstrated severe degeneration. Possibly, unrelated genetic interactions complicated matters. We therefore focused all of our efforts on mice expressing Bouse heterozygously on a WT background (i.e., Bouse+/−, R+/+), which will hereafter be referred to as Bouse mice.

Protein analyses

Retinas from dark-adapted Bouse and WT mice aged 6–9 weeks were homogenized in a protease solution (Complete Mini, EDTA-free, Roche Diagnostics, Indianapolis, IN). Rhodopsin content was determined spectrophotometrically. Homogenates were suspended in sample buffer containing 30% glycerol, 6% sodium dodecyl sulfate, 0.05% bromophenol blue (Sigma, St. Louis, MO), 3 mM dithiothreitol, and 70 mM Tris chloride, pH 6.8; and a series of rhodopsin concentrations was loaded onto a polyacrylamide gel. Proteins were separated by electrophoresis, transferred to membranes (Immobilon-FL, Millipore, Billerica, MA), and probed with antibodies: anti-rhodopsin (1:2000, PA1-729, Affinity Bioreagents, Golden, CO), anti-rds/peripherin (1:500, provided by G. Travis, Jules Stein Eye Institute, Los Angeles, CA), anti-transducin α-subunit (1:1000, sc-389, Santa Cruz Biotechnology, Santa Cruz, CA), anti-transducin β-subunit (1:1000, sc-379, Santa Cruz Biotechnology), anti-arrestin (1:300 or 1:500, PA1-731, Affinity Bioreagents), anti-rhodopsin kinase (1:500, MA1-720, Affinity Bioreagents), anti-PDE α- and β-subunits (1:10,000, PatB provided by RW Lee, University of California at Los Angeles or 1:1000, PAB-06800, Cytosignal, Irvine, CA), anti-phosducin (1:50,000, GertieB) (18), anti-recoverin (1:50,000, P26) (19), anti-RGS9 (1:1000, provided by T. G. Wensel, Baylor College of Medicine, Houston, TX), anti-rootletin (1:4000, anti-root6) (20), anti-AIPL1 (1:2000) (21), and anti-ABCR (1:30, Rim3F) (22). The epitope recognized by the PA1-729 antibody for rhodopsin was shared in native mouse rhodopsin and Bouse rhodopsin. Membranes were treated with horseradish peroxidase-conjugated secondary antibody and a chemoluminescent substrate (Pierce Biotechnology, Rockford, IL) and exposed to x-ray film, which was read with a densitometer (Storm 860 with ImageQuaNT software, Molecular Dynamics, Sunnyvale, CA). In later experiments, the horseradish peroxidase-conjugated secondary antibody was substituted with fluorochrome-conjugated goat anti-rabbit IgG (1:5000, IRDye800; Rockland Immunochemicals, Gilbertsville, PA) and probed with an infrared fluorescence reader (Odyssey, LI-COR Biotechnology, Lincoln, NE). After adjusting for background, band density or fluorescence was plotted as a function of the amount of rhodopsin loaded, and the relations were fit by linear regression to compare the slopes of Bouse and WT samples. Each protein was tested on three to nine different sample pairs, in which a sample typically consisted of four retinas from two Bouse mice or two retinas from a WT mouse. Although the ratios are given in the text and figure for simplicity, the analysis of variance followed by a Sidak posthoc test were performed on $\log_{10}(\text{slope}_{\text{Bouse}}/\text{slope}_{\text{WT}})$ to minimize distortions in the population distributions caused by the use of ratio transformations. P-values <0.05 were considered to be significant.

Analysis of fatty acids in disk membranes

Bouse and WT mice were dark-adapted for a minimum of 12 h. Retinas were removed and disk membranes were prepared according to Calvert et al. (14). Lipids were extracted and fatty acids were derivatized as described in Makino et al. (23). The fatty-acid compositions were determined by gas-liquid chromatography; 3 μl of each sample were injected at 250°C with a split ratio of 10:1 onto a DB-225 capillary column (30 m × 0.32 mm I.D.; J&W Scientific, Folsom, CA) in an Agilent 6890N gas chromatograph with model 7683 autosampler (Agilent Technologies, Wilmington, DE). The column temperature was programmed to begin at 160°C, ramped to 220°C at 1.33°C/min, and held at 220°C for 18 min. Hydrogen carrier gas flowed at 1.6 ml/min, and the flame ionization detector temperature was set to 270°C. The chromatographic peaks were integrated and processed with ChemStation software (Agilent Technologies). Fatty-acid methyl esters were identified by comparison of their relative retention times with authentic standards (NU-CHEK PREP, Elysian, MN). Relative mole percentages were calculated and compared by analyzing the variance and by utilizing a Sidak posthoc test.

Suction electrode recording

Photoresponses were recorded from single rods by the suction electrode method as described in Liu et al. (21). Seven Bouse and four control mice, aged 5–9 weeks, were kept in darkness overnight before an experiment. Retinas were placed in chilled, oxygenated Leibovitz's L-15 medium and the vitreous removed. A piece of retina was chopped finely, and the pieces were loaded into an experimental chamber. The tissue was perfused with an enriched Locke's solution (mM): 139 Na^+, 3.6 K^+, 2.4 Mg^{2+}, 1.2 Ca^{2+}, 123.3 Cl^-, 20 HCO_3^-, 10 HEPES, 3 succinate, 0.5 L-glutamate, 0.02 EDTA, and 10 glucose, supplemented with 0.1 mg/ml bovine serum albumin (Fraction V, Sigma), 1% by volume of minimal essential medium amino acids (Invitrogen, Carlsbad, CA), and 1% by volume of basal medium Eagle vitamins (Sigma), warmed to 37°C. The outer segment of a single rod was pulled into a glass pipette to record responses to flashes (nominally 20 ms in duration) with a patch clamp amplifier (Axopatch 200A, Axon Instruments, Union City, CA). The pipette was filled with HEPES buffered Locke's that lacked amino acids and vitamins and replaced bicarbonate with Cl^-. The light, from a xenon source, passed through a 500 nm interference filter, and its intensity was adjusted with neutral density filters. Responses were low-pass filtered at 30 Hz (-3 dB, 8-pole Bessel, Frequency Devices, Haverhill, MA) and digitized at 400 Hz on a MacIntosh computer (Pulse, version 8.07, HEKA Elektronik, Lambrecht, Germany). In some cases, records were digitally filtered at 12 Hz by convolution with a Gaussian (Igor Pro version 5.03, WaveMetrics, Lake Oswego, OR). Responses were also recorded on videocassette after filtering at 1 kHz (4-pole Bessel on Axopatch amplifier), using a pulse code modulator (Neuro-corder DR-484, Neuro Data Instruments Corporation, Delaware Water Gap, PA). Some of these recordings were redigitized at 1 kHz after low-pass filtering at 80 Hz (8-pole Bessel) and then digitally filtered at 34 Hz for the determination of the amplification constant. The analysis was restricted to responses near saturation: $0.6\, r_{\max} < r < r_{\max}$. No corrections were made for the delays of ~17 ms or 6 ms introduced by low-pass filtering at 30 or at 80 Hz, respectively. Digital filtering smoothed the waveform without introducing any delay.

For the analysis of Na^+/Ca^{2+}, K^+ exchange currents, a line was fit to the rising phase of a saturating response starting from ~0.25 $r_{\max}$ up to the time point when the response deviated substantially from linearity. Thereafter, the response was fit with a single exponential function with an offset (Igor Pro).

The range of the exponential fit extended for a minimum of ~2 time constants to no more than ~5 time constants. Amplitude of the exchange current was taken as the value extrapolated to the time when the saturating flash response was half maximal.

Electron microscopy

Eyes from 6-weeks-old Bouse and 6–9 weeks old WT mice were enucleated, cleansed of extraneous tissues, and immersed in modified Karnovsky's fixative consisting of 2.5% gluaraldehyde and 2% formaldehyde in 0.1 M cacodylate buffer containing 0.08 M $CaCl_2$, at 4°C for 20–24 h. Eyes were washed in 0.1 M cacodylate, post-fixed in 2% aqueous OsO_4, dehydrated with a graded series of ethanol, transitioned to propylene oxide, and embedded in TAAB Epon resin. Blocks were sectioned at 70–90 nm, stained with uranyl acetate and Sato's lead stain, and viewed on a Philips CM-10 electron microscope (Eindhoven, The Netherlands). The rod outer-segment diameter was determined from sections taken tangential to the retina, whereas the spacing between disks was determined from longitudinal sections on which the rims of at least 24 consecutive disks could be discerned. Measurements of rod diameter and disk spacing were made on rods from two mice of each type.

Microspectrophotometry

Retinas from three Bouse mice, aged 6–7 weeks, and three WT mice, aged 5–8 weeks, were isolated into bicarbonate buffered Locke's solution containing 0.1 mg/ml bovine serum albumin and 10 mM glucose. A sample was chopped in Locke's containing 2% methylcellulose on a glass coverslip that had been coated previously with poly-l-lysine. Poly-l-lysine and methylcellulose discouraged unwanted motion of the rods (24,25). The sample was encircled with silicone oil and a second coverslip was placed on top. Quartz coverslips (Electron Microscopy Sciences, Hatfield, PA) were used in a few experiments. The preparation was mounted on the stage of the Williams-Webbers microspectrophotometer (26), equipped with two 100× quartz objectives (Ultrafluar, Zeiss). A piezoelectric device under computer command adjusted the stage height automatically to correct for chromatic aberration. A baseline reading was taken with the measuring beam (nominally 0.5 × 2.5 μm) placed in a cell-free area. The beam was then relocated on the outer segment of a single rod for a second reading. The measuring beam was polarized, with the electric vector positioned perpendicular to the long axis of the outer segment, for optimal photon absorption. Absorbance was calculated online. Scans were taken two at a time to allow for frequent checks of the beam alignment. An individual rod was scanned no more than six times, and measurement bleached negligible amounts of rhodopsin. Wavelength was calibrated by scans through a holmium oxide standard (CRM100, SpectroStandards, Fort Collins, CO).

RESULTS

Analysis of protein expression

Flash-response sensitivity and kinetics are sensitive to the concentrations of key phototransduction proteins (27). Regulatory control over their expression levels is not well understood, and therefore it was important to find out whether Bouse expression caused any changes. Rod proteins were probed by immunoblotting, in which the amount of protein was plotted against the amount of rhodopsin loaded onto the gel, and the slope was determined over the linear range (Fig. 1, *A–C*). The ratio of the slopes, transgenic divided by WT, served as an estimate of the protein ratio. Control experiments on rod opsin yielded a ratio of 0.96, close to the expected value of unity. Sizeable fractions of some phototransduction proteins, such as arrestin and recoverin, localize in the inner segments of dark-adapted rods (19,28,29). Had a significant number of Bouse rods lost their outer segments, ratios for inner-segment proteins would have increased due to an enrichment of these phototransduction proteins relative to rhodopsin in WT retinas. Such ratios would not be representative of phototransducing rods, and, therefore, we included two inner-segment-specific proteins, AIPL1 and rootletin (20,30), and two outer-segment-specific proteins, ABCR and rds/peripherin (31,32), to investigate the issue. No differences in the ratios between these outer- and inner-segment proteins were found. Although it is possible that Bouse rods without outer segments expressed less AIPL1 and rootletin, it is more likely that few Bouse rods were missing their outer segments. The ratios for the majority of the proteins—transducin α-subunit, transducin β-subunit, PDE catalytic subunits, GRK1, arrestin, RGS9, rds/peripherin, and AIPL1—were not different from each other (Fig. 1 *D*). But, collectively, the mean ratio for this select subset of proteins was lower than the ratio for opsin ($p < 0.001$). The ordinate on the right side of Fig. 1 *D* scales the ratio for each protein by the mean ratio for the selected subset of proteins to provide perspective on the relative expression levels. Barring an overall decrease in the synthesis of all proteins with the exception of opsin, our analyses indicated a 1.5-fold overexpression of opsin in Bouse rods. The ratio for recoverin of 0.92 did not differ significantly from that for the selected subset of proteins listed above.

The ratio for phosducin of 0.43 was less than the values for opsin ($p < 0.001$), recoverin ($p < 0.002$), rootletin ($p < 0.007$), ABCR ($p < 0.003$), and the selected subset of proteins ($p < 0.013$). Because rhodopsin expression was 1.5-fold higher in Bouse mice, the relative phosducin expression was 0.7 of that in WT mice (Fig. 1 *D*).

Unperturbed fatty-acid composition of Bouse disk membranes

Increased phospholipid/rhodopsin ratio in R +/− mice (14) suggested that increased opsin expression might lower phospholipid/rhodopsin ratio in Bouse mice. However, the fatty-acid composition of Bouse disk membranes was similar to that in WT and to previous characterizations of WT mice (14,23,33). The molar phospholipid/rhodopsin ratio for Bouse was 62 ± 7 (mean ± SE, $n = 6$), whereas the ratio for WT was 59 ± 14 ($n = 6$). The distributions of all fatty acids comprising more than 2% of the membrane were similar in Bouse and WT preparations (Fig. 2). Accordingly, the ratio of n6 to n3 fatty acids was conserved (Fig. 2), the mean fatty-acid length in the disk membranes of both types of mice was 19 carbons, and the average number of double bonds per fatty acid was 2.7 ± 0.1 for Bouse and 2.8 ± 0.2 for WT. These results were not consistent with an increase in the packing density of rhodopsin in Bouse rods or with a change in the intrinsic fluidity of the disk membrane.

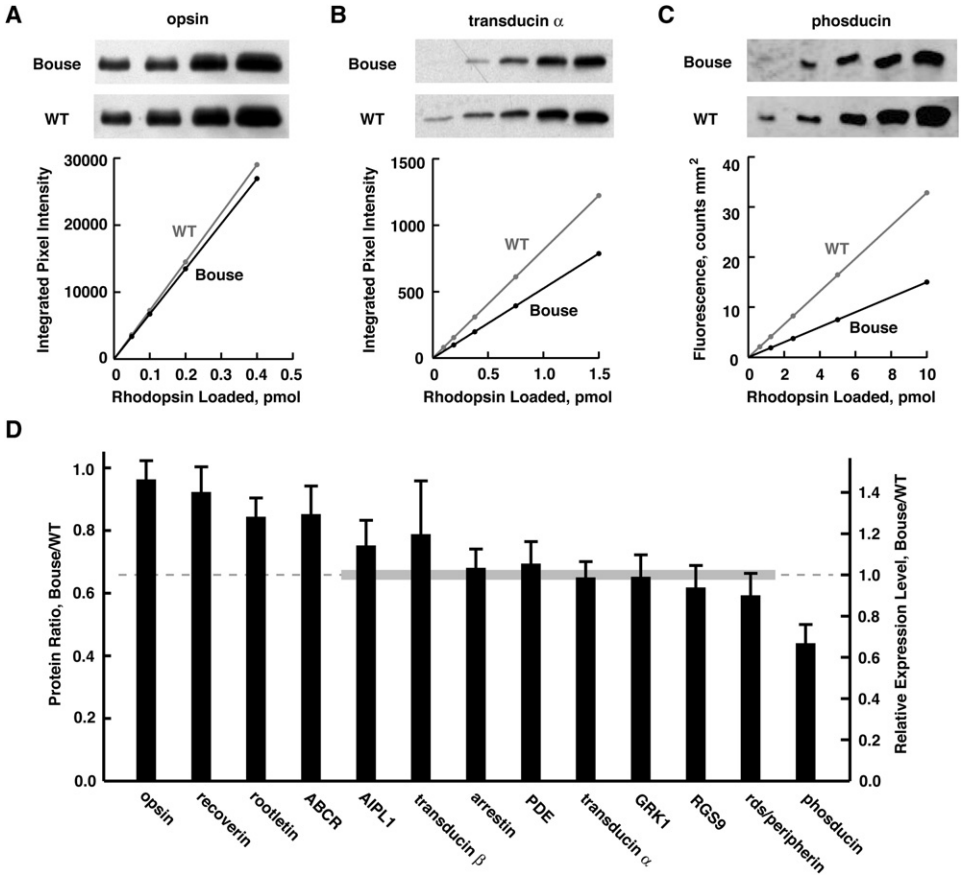

FIGURE 1 Measurements of rod proteins. (*A–C*) Immunoblots of opsin, transducin α-subunit, and phosducin with plots of results (*lower panels*) for Bouse rods (*black*) and WT rods (*gray*). Opsin and transducin were quantified by densitometric scanning, whereas phosducin was probed with fluorescence (see Methods). Continuous lines show fits by linear regression, constrained to pass through the origin. (*D*) The expression of each protein is plotted as the ratio of the slope from Bouse divided by the slope from WT. Error bars are SE, $n = 3$–9 sample pairs. The dashed gray line shows a selected subset of proteins (*bold gray line*): AIPL1, transducin α- and β-subunits, arrestin, PDE, GRK1, RGS9, and rds/peripherin, for which the antilog of the mean $\log_{10}(\text{slope}_{\text{Bouse}}/\text{slope}_{\text{WT}})$ value was set to 1 to compare the relative expression level of Bouse to WT (*right ordinate*). WT, wild-type.

Modifications in Bouse rod outer-segment ultrastructure

In general, Bouse rod outer segments were short and gnarled with frequent vesiculations and swollen areas of disordered disk membranes. Overall, the degeneration seemed more advanced than that described by Tan et al. (16), perhaps because the Bouse rods in this study expressed higher levels of opsin than did those expressed in the original study. The time-course and severity of disruption may have also varied with genetic background (see Methods). A small population of rods with relatively good preservation of outer-segment structure at the light-microscopic level was subjected to further scrutiny by microspectrophotometry, electrical recording, and electron microscopy. Bouse rod outer segments with regular arrays of neatly arranged disks (Fig. 3) had a disk-to-disk repeat distance of 317 ± 5 Å ($n = 16$), similar to that in WT rods, 321 ± 4 Å ($n = 73$). Our value for WT, although greater than that observed by Carter-Dawson and LaVail (34), was comparable to other published values (15,23,35).

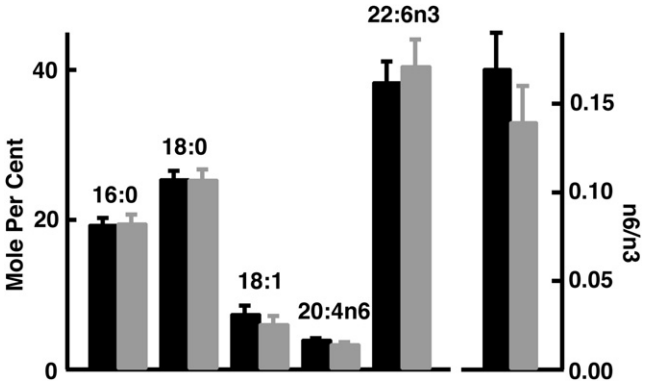

FIGURE 2 There was no change in the fatty-acid composition of disk membranes in Bouse rods. The mole percentages of each of the major fatty acids (*left panel*) and the ratio of n6 to n3 fatty acids (*right panel*) are plotted for Bouse (*black*) and WT (*gray*) disk membranes. WT, wild-type.

Cone outer-segment diameters tend to be smaller than those of rods, and cones taper with distance from the inner segment. Although cones comprise only ~4% of the outer-segment pool (34), we minimized their contribution to the determination of WT rod outer-segment diameter further by restricting measurements in cross sections to profiles with a single incisure (Fig. 3 *D*), because the membranous sacs of cones may have several incisures, whereas mouse rod disks have only one (34,36). Cross sections of all Bouse rods exhibited prominent striations (Fig. 3 *C*). Some WT rods also had striations, but the incidence was lower. Our interpretation is that Bouse disks were seldom if ever aligned perpendicular to the outer-segment axis and that the angle of slant was more pronounced than in WT. Incisures were not

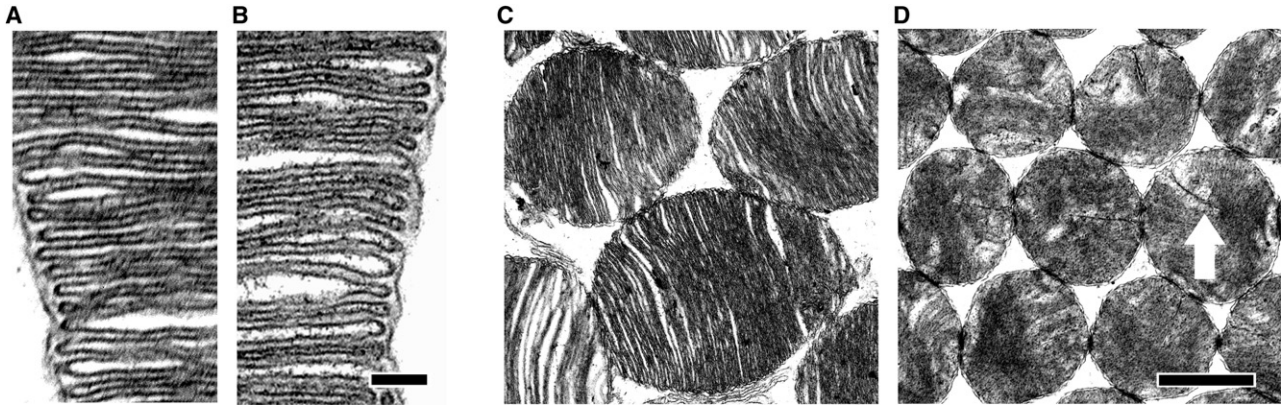

FIGURE 3 Structure of Bouse outer segments. For Bouse rods retaining an orderly stacking of membranes in their outer segments (*A*), disk membrane spacing in longitudinal sections was similar to that in WT rods (*B*). In tangential sections, the diameter of Bouse rods (*C*), was larger than that of WT (*D*). Lamellae coursed across Bouse rods viewed in cross section, giving them a more striated appearance. Long incisures (*arrow*) were only observed in WT rods. Scale bars: 0.1 μm in *B* applies to panels *A* and *B*, 1 μm in *D* applies to panels *C* and *D*. WT, wild-type.

detected in Bouse cross sections and were rarely seen in Bouse longitudinal sections. For WT rods, the outer segment diameter of 1.351 $\pm$ 0.006 μm ($n = 299$) was similar to that in previous reports (15,23,34), whereas, in Bouse rods, diameter was enlarged to 1.73 $\pm$ 0.03 μm ($n = 74$, $p < 0.0001$). The value for Bouse rods represents a lower limit, because frequently encountered misshapen rods and rods with vesiculated or disorganized membranes were larger, but were excluded on the grounds that they were unlikely to have been selected for recording.

Increased transverse absorbance of Bouse rods

Absorbance of individual rod outer segments was measured side-on with a microspectrophotometer. Spectra for some of the rods are shown in Fig. 4. The spectral maximum obtained from template fits to individual rods (37) was 505 nm for Bouse and WT rods. The absorbance of 0.0123 $\pm$ 0.0005 for 27 Bouse rods was greater than the absorbance value of 0.0104 $\pm$ 0.0003 for 62 WT rods ($p < 0.003$). The small size of mouse rods precluded accurate measurement of the diameter of each rod with our infrared imaging system during the study. Taking mean diameters from electron microscopy, the specific absorbances of Bouse and WT rods were 0.007 μm^{-1} and 0.008 μm^{-1}, respectively. The WT specific absorbance was somewhat low for mouse rods (7), perhaps due to imperfect focusing of the measuring beam on such small cells. It is noteworthy that Bouse and WT specific absorbances did not differ from each other. Specific absorbance at 500 nm is proportional to the rhodopsin concentration, and, therefore, given that the separation of disk membranes was normal in Bouse rods (Fig. 3, *A* and *B*), the rhodopsin packing in those membranes was also normal.

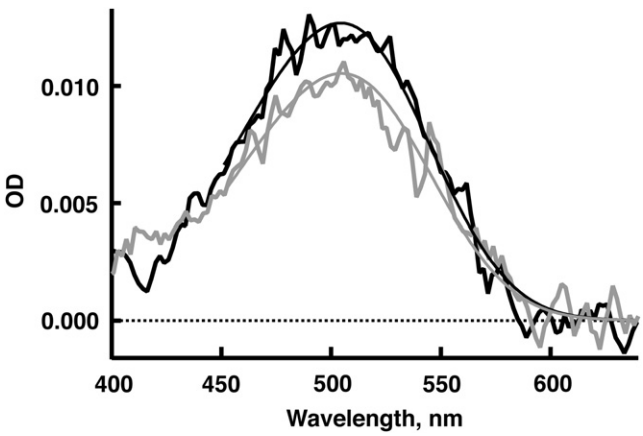

FIGURE 4 Increased absorbance of Bouse rod outer segments compared to those of WT rod. Spectra are averages of eight Bouse rods (*thick black trace*) and 24 WT rods (*thick gray trace*). Thin lines show A_1-based template fits (37). WT, wild-type.

Altered flash responses in Bouse rods

In contrast to the thin WT rods, thick Bouse rods probably sealed more tightly in the suction electrode. Consequently, outer-segment membrane currents were collected more efficiently from Bouse rods, which would have made their recorded photoresponses proportionately larger (Fig. 5 *A*; Table 1). The expanded Bouse rod diameter also improved photon capture, which enhanced the relative sensitivity (Fig. 5 *B*; Table 1). Although the larger circumference of Bouse rods would have increased total membrane capacitance, the relatively small change in the submillisecond time constant for rods (38) would have had little effect on response kinetics.

The mean amplitude of the single-photon response, a, was estimated by dividing the ensemble variance, σ^2, by the mean amplitude, r_d, for responses elicited by dim flashes (39):

$$a = \sigma^2 / r_d. \quad (1)$$

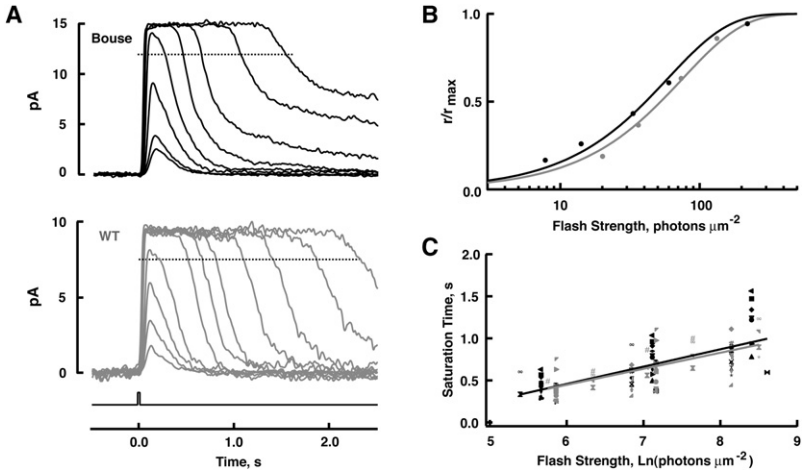

FIGURE 5 Flash-response properties of a Bouse rod (*black traces* and *symbols*) and a WT rod (*gray traces* and *symbols*). (*A*) Averaged responses of a Bouse rod (*upper panel*) and a WT rod (*lower panel*) to flashes. Flash strengths were: 7.8, 14.1, 33.3, 60.1, 220, 940, 3440 and 14700 photons μm^{-2} for Bouse and 20.1, 36.3, 73.7, 133, 568, 1150, 2080, 4920, 8880, 18000, and 32500 photons μm^{-2} for WT. Records were digitally filtered at 12 Hz. (*B*) Stimulus-response relations for the rods from A; for illustrative purposes, not all points were plotted. Results were fit with a saturating exponential function, $r/r_{max} = 1-\exp(-ki)$, where i is flash strength, k is equal to $\ln(2)/i_{0.5}$, and $i_{0.5}$ is the flash strength that produces a half-saturating response. (*C*) Pepperberg plot for 22 Bouse (*black*) and 18 WT (*gray*) rods. The saturation time of a bright-flash response was measured from midflash to the point at which the response declined to 0.8 r_{max}, that is, 20% recovery, as demarcated by the dotted lines in *A*. Values for τ_c, given from linear regression (*continuous lines*), were 206 ms for Bouse and 191 ms for WT. The Pearson product-moment correlation coefficients for Bouse and WT rods were 0.677 and 0.656, respectively. WT, wild-type.

The Bouse response peaked later than did the WT single-photon response, and it eventually reached an amplitude that was 1.5 times larger (Fig. 6 *A*; Table 1). Because the difference in amplitude was likely to have resulted in part from improved current collection in the Bouse recordings, the fractional response was found by dividing the single photon response by the r_{max} for each rod. However, r_{max} varies with rod outer-segment length, which was shorter in Bouse rods. Single-photon response amplitude in pA was not affected by outer-segment length over the range encountered in these rods, and so it was necessary to normalize by a length factor, L, to compare fractional responses. Because photon-collecting area A_c, taken as

$$A_c = r_d^2/\left(i_d\sigma^2\right), \quad (2)$$

is proportional to outer-segment volume, L equals the outer segment length, λ, for a given rod relative to the mean wild-type value:

$$L = \lambda/(\lambda_{\text{mean WT}}) = (A_c/A_{c\ \text{mean WT}})(d_{\text{WT}}/d_{\text{Bouse}})^2. \quad (3)$$

Using calibrated flash strengths for i_d and disk diameters, d, from Table 1, Bouse rod outer segments were on average 0.7 as long as were WT rod outer segments. After multiplying the single-photon responses by L, the normalized, fractional amplitudes were similar for Bouse and WT rods (Fig. 6 *B*; Table 1). The Bouse response rose more gradually than did the normal response, after an initial delay of ~3 ms (Fig. 6 *C*). After a slower initial recovery near the peak, the Bouse response soon declined exponentially with the same time constant as that in WT (Fig. 6 *D*; Table 1).

A biophysical model (40) that took into consideration the effect of different geometries and the localized effects of a photoisomerization within the layered structure of the outer segment showed that the increase in outer-segment diameter and removal of the incisure delayed the single-photon response, reduced its rate of rise, and lowered its overall amplitude (Fig. 7 *A*, *thick black trace*). Two primary effects were at play: i), the concentrations of transducin and PDE were reduced, and so the intermolecular collision rates were slowed and ii), cGMP depletion had to occur over

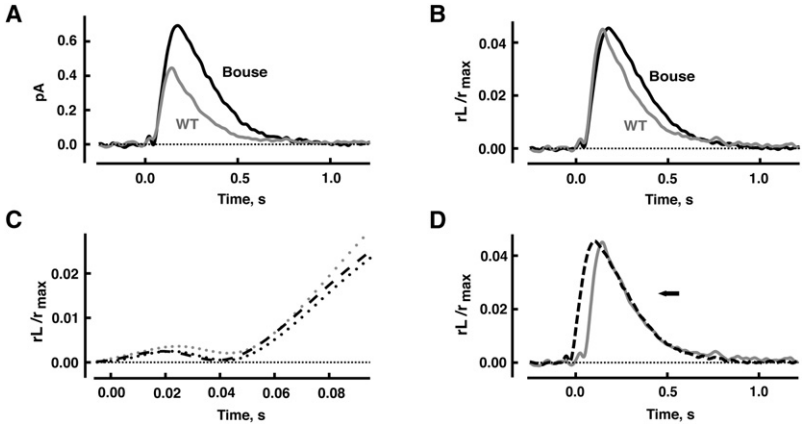

FIGURE 6 Slower rise of the single-photon response in Bouse rods. (*A*) The mean dim-flash response from each rod was scaled to the amplitude of the single-photon response. Then, averages were taken for 10 Bouse rods (*black*) and 12 WT rods (*gray*). Traces were digitally filtered at 12 Hz. (*B*) Normalized fractional response. Single-photon responses of each rod of a given type were adjusted by an outer-segment length factor, L, divided by the saturating-response amplitude for that rod and then averaged. (*C*) Rising phases of the responses in *B* on an expanded timescale, showing the delayed onset of the Bouse response. Dashed line shows the Bouse response shifted to the left by ~3 ms. (*D*) Normal recovery of the Bouse quantal response. The Bouse response (*dashed trace*) was translated on the time axis for alignment to the WT response. WT, wild-type.

TABLE 1 Flash-response properties and outer-segment dimensions of Bouse rods versus WT rods

Variable	Bouse rods*	WT rods	*P*-value†
Circulating current (pA)	10.1 ± 0.5, 35	8.3 ± 0.4, 23	<0.009
$i_{0.5}$ (photons μm^{-2})	38 ± 2, 31	51 ± 3, 23	<0.0003
Single-photon response			
Amplitude (pA)	0.72 ± 0.07, 10	0.47 ± 0.06, 12	<0.016
Normalized fractional amplitude	0.055 ± 0.005, 10	0.047 ± 0.005, 12	Ns‡
Time to peak (ms)	167 ± 8, 22	138 ± 10, 17	<0.03
Integration time (ms)	336 ± 19, 22	267 ± 32, 17	Ns
Recovery time constant (τ_r, ms)	228 ± 24, 22	177 ± 23, 16	Ns
Amplification constant (A, s^{-2})	29 ± 6, 10	47 ± 7, 11	Ns
Saturation time constant (τ_c, ms)	206, 22	191, 16	—
Na^+/Ca^{2+}, K^+ exchange			
Time constant (ms)	51 ± 6, 24	56 ± 14, 13	Ns
Fractional amplitude	0.12 ± 0.01, 24	0.11 ± 0.02, 13	Ns
Rod outer-segment diameter (μm)	1.73 ± 0.03, 74	1.351 ± 0.006, 299	<0.0001
Disk-to-disk repeat distance (Å)	317 ± 5, 16	321 ± 4, 73	Ns

Flash-response properties of Bouse rods were determined by single-cell recording. $i_{0.5}$ indicates the flash strength eliciting a half-maximal response, varying inversely with sensitivity. Single-photon response amplitude was estimated by dividing the ensemble variance by the mean dim flash-response amplitude. To obtain normalized, fractional amplitude, the single-photon response was divided by the circulating current and then multiplied by a factor to account for the difference in outer-segment length (see text). Kinetics of the single-photon response were determined from dim flash responses whose amplitude was less than one-fifth of the maximum. Time to peak was measured from midflash to the response peak. Integration time was calculated as the integral of the response divided by response amplitude. Recovery time constant refers to a fit of the final falling phase of the dim flash response with a single exponential. Amplification constant was calculated from Eq. 4. Saturation time constant was the slope of the relation between saturation time and the natural logarithm of the flash strength, by linear regression as illustrated by the scatter plot in Fig. 5 *C*. Parameters for Na^+/Ca^{2+}, K^+ exchange were obtained from fits to saturating flash responses, as described in Methods. Rod outer-segment dimension was measured by TEM.

WT, wild-type.

*Values are given as mean ± SE, number of rods analyzed.

†*P*-values were obtained from two-tailed *t*-tests.

‡Ns indicates $p > 0.05$, deemed to be not significant.

a greater volume. The simulated Bouse response was then multiplied by a factor to reproduce the higher current collection efficiency during recording (Fig. 7 *A*, *thin black trace*). After dividing by the respective circulating currents and scaling by *L* to adjust for the shorter outer-segment length in Bouse rods, the slower rise and the lower amplitude in the simulated Bouse response were accentuated, compared to the recorded response (Fig. 7 *B*). Raising the density of channels in the plasma membrane (not shown) or boosting the overall guanylyl cyclase density on the disk membrane to WT levels (Fig. 7 *C*) increased the single-photon response amplitude in pA and the circulating current but made the normalized fractional Bouse response only slightly larger (Fig. 7 *D*). Boosting guanylyl cyclase

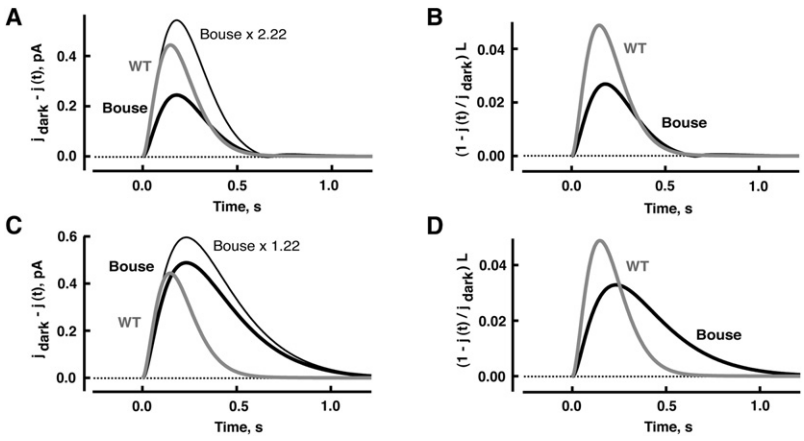

FIGURE 7 Simulation of the Bouse (*black*) and WT (*gray*) single-photon responses predicted by the localized effects model of Bisegna et al. (40), where j_{dark} is the circulating current in darkness and $j(t)$ is the time-varying circulating current. Outer-segment diameter was 1.73 μm for Bouse and 1.35 μm for WT. A single incisure whose length spanned 0.409 of the diameter of the disk was included for the WT rod, whereas the incisure was omitted for the Bouse rod. Outer-segment length for the Bouse rod was set to 0.7 of the length of the WT rod. The Bouse rod contained 1.5 times as much rhodopsin per unit length as did the WT rod. For one set of simulations (*A* and *B*), the numbers of copies of other phototransduction proteins per disk and the number of CNG channels per unit length were held constant at the wild-type values. For a second set of simulations, the numbers of guanylyl cyclases and CNG channels were increased so that the rate of cGMP synthesis per unit volume and the membrane density of the channels were normal (*C* and *D*). In the plots of current drop in pA, the Bouse trace included a multiplicative scaling factor (2.22 in *A*, 1.22 in *C*) to allow for an increase in current recording efficiency in the experimental setting (see text). Normalized fractional responses for each set of conditions (*B* and *D*) were computed from the corresponding responses in pA (*A* and *C*). *L* was set to the appropriate mean value for the rods in Fig. 6 *B*: 0.7 for Bouse and 1.0 for WT. The j_{dark} values for Bouse, uncorrected for differences in current collection efficiency, were 6.4 pA in *A* and 10.4 pA in *C*, whereas, for WT, j_{dark} was 9.1 pA. WT, wild-type.

activity also slowed down the recovery phase. A more complete description of the modeled response will appear in a future publication.

Bright flashes saturate the response in which the duration spent in saturation increases linearly with the natural logarithm of the flash strength (41). The slope of the relation, τ_c, estimates the time constant for the decay in PDE activity (41,42), which is predominated by the lifetime of activated transducin (43). τ_c was unaffected by the expression of the Bouse transgene (Fig. 5 *C*; Table 1), indicating that the rate of transducin shutoff was preserved. By inference, the rate of rhodopsin quench, as a nondominant step in the photoresponse recovery, could not have been greatly slowed.

The rising phases of bright-flash responses were characterized by an amplification factor, *A*, that relates the rapidity with which the photoresponse develops to the number of photoisomerizations (44):

$$r/r_{\max} = \left(1 - \exp\left(-0.5\Phi A\left(t - t_{\text{eff}}\right)^2\right)\right) \text{for } t > t_{\text{eff}}, \quad (4)$$

where t_{eff} is a latency and Φ is the number of photoisomerizations per flash. Here, Φ was found by multiplying collecting area from Eq. 2 by flash strength. The analysis was restricted to responses that were near saturation, because signal-to-noise was better and because they rose too quickly for cascade feedback to have a major influence on the responses (Fig. 8). The amplification factor for WT rods (47 ± 7 s^{-2}, $n = 11$) was somewhat higher than that reported for mouse rods by others (14,23,45), possibly due to uncertainties in the estimation of Φ. Notably, though, the mean value for Bouse rods (29 ± 6 s^{-2}, $n = 10$) was 1.6-fold lower than that for WT ($p < 0.06$).

The light-induced fall in intracellular Ca^{2+} shapes the photoresponse by exerting a powerful control over guanylyl cyclase activity. Ca^{2+} dynamics were probed with bright, saturating flashes (46). The steep rise of the response due to CNG channel closure gave way to a slower phase that reflected the action of the Na^+/Ca^{2+}, K^+ exchanger. Removal of Ca^{2+} is coupled to the stoichiometric entry of four Na^+ and departure of one K^+ (47). Hence, there is a net inward charge movement during each cycle. The exchange current followed an exponential time course, as intracellular Ca^{2+} dropped to a minimum. The time constant for the exchange current decline in WT of 50 ms (Table 1) was slightly faster than that previously reported (14,48,49), perhaps due in part to differences in the fitting procedure (see Methods). However, the time constant as well as the initial amplitude of the exchange current, normalized for circulating current, were similar for Bouse and WT rods (Table 1), suggesting that Ca^{2+} feedback operated normally in Bouse rods.

DISCUSSION

The high density of rhodopsin in the outer-segment disks, ~25,000 μm^{-2} (8,35), promotes photon capture but interferes with downstream reactions in the phototransduction cascade by impeding the lateral diffusion of all proteins on the membrane (10). Underexpression of rhodopsin relieves protein crowding (7,14), and therefore overexpression was expected to exacerbate it. Tan et al. (16) inserted a transgene for a rod opsin into the mouse genome and produced several lines of mice with increased rhodopsin expression. The Bouse A line was described as having a 1.23-fold increase in opsin based on ELISA of opsin and rds/peripherin and the assumption that expression of the latter was unchanged, and a 26% increase in 11-*cis* retinal content in its retina. In our colony of Bouse A mice, we observed 1.3–1.5-fold overexpression of rhodopsin based on Western blot analyses of a greater number of rod proteins and on independent studies of microspectrophotometric and electron microscopic measurements (Figs. 1–4). However, microspectrophotometric determinations of specific absorbance in Bouse rods revealed that the concentration of rhodopsin in their disks was normal. The lowered packing density of rhodopsin in R+/− disk membranes increased the phospholipid/rhodopsin ratio (14), and so any increase in rhodopsin packing density in Bouse should have had the opposite effect. Yet, in Bouse disk membranes, the phospholipid/rhodopsin ratio was normal. Evidently, the increased expression of rhodopsin in Bouse led to an expansion of the outer-segment diameter (Fig. 3) without a change in the packing density of rhodopsin. Thus, we propose that there is a coupling between the amount of rhodopsin arriving at the outer segment, and the formation and size of outer-segment disks, which affects the rod's function in phototransduction. Although the nature of this coupling is not yet known, it points to a need for a clearer cell biologic understanding of how formation, geometry, and function of photoreceptors are linked. A simple mechanism may involve the obligatory association of a minimal amount of lipid with each rhodopsin molecule transported along the cilium during the construction of nascent disks (50,51). There may be some flexibility

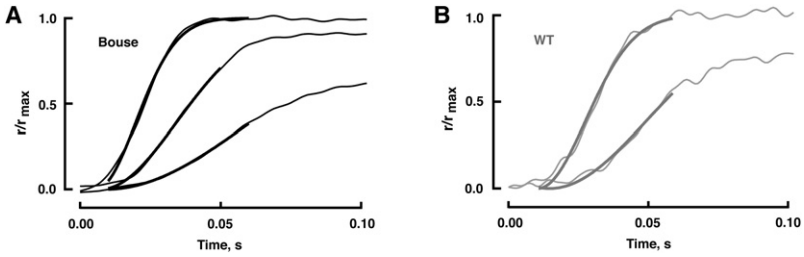

FIGURE 8 Reduced amplification of Bouse flash responses. Responses (*thin lines*) were fit with Eq. 4 (*thick lines*). (*A*) Averaged Bouse responses to flashes of 60.1, 220, and 940 photons μm^{-2}. The amplification constants were 28, 29, and 29 s^{-2}, respectively. (*B*) Averaged WT responses to flashes of 82.2 and 351 photons μm^{-2}. The amplification constants were 35 and 37 s^{-2}. WT, wild-type.

to increase the amount of lipid per rhodopsin if necessary, because the phospholipid/rhodopsin ratio increases and outer-segment absorbance decreases in R+/− rods (7,14) and in rods of albino rats raised in bright light (4,5). Decreasing the amount of lipid per rhodopsin may not be an option in general, although rods of certain deep-sea-dwelling fish exhibit a high specific absorbance (52,53) and could represent an exception if rhodopsin is indeed more densely packed in their disk membranes. These fish may have developed special adaptations during their evolution to enable them to cope with extreme conditions. It would then be worthwhile to study the impact of these adaptations on phototransduction.

Potentially, the scaled-up production of rhodopsin in Bouse rods may have decreased the expression of other proteins—by a diversion of resources, for example. A deficiency in rom1 may have led to disk expansion and disorganization, because rods of mutant ROM1−/− and ROM1+/− mice share the large-disk phenotype with the Bouse line (54). Rds/peripherin and rom1 are integral membrane proteins of the tetraspannin family that form heterotetramers thought to help shape and support the hairpin turn in the membrane rims of the disk perimeter and incisure (55). Binding of the complex to soluble, glutamic acid-rich proteins (GARPs) and to the GARP domain of CNG channels may provide a means for anchoring disks to each other and to the plasma membrane, to stabilize the stack of disks (35). Another, more intriguing, possibility is that increased rhodopsin production in Bouse rods relieved a constraint on disk growth and that constancy of rds/peripherin expression in the face of increased girth in Bouse outer segment may have precluded incisure formation because of an inadequate rds/peripherin supply. The circumference of Bouse outer segments with well-organized disks in cross section was 1.73π μm, approximating the circumference of WT outer segments plus the length of an incisure (incisures extend nearly halfway across a WT diameter, Fig. 3). As Bouse disk diameters surpassed 1.7 μm, the supply of rds/peripherin was no longer sufficient to maintain proper membrane organization of the disk rim, and so these rods were filled with disrupted disks. The failure of homozygous rds mice to form outer segments and the abnormalities in disk formation and structure arising in heterozygous rds mice, transgenic mice expressing mutant rds/peripherin, rom1 knockout mice (55), and mice after knockdown of an intraflagellar transport protein that seems to affect the localization of rom1 to the outer segment (56) are consistent with this view. Because a dose-dependent rescue was achieved upon transgenic replacement of the faulty rds/peripherin in rds mice (57), raising the expression of rds/peripherin may ''correct'' the outer-segment structure and preserve rods in Bouse mice.

Despite the normal rhodopsin packing density in the membrane, flash responses were changed in Bouse rods. The normalized, fractional Bouse single-photon response was delayed and then rose more gradually than did the WT response (Fig. 6). Genetic ablation of phosducin reduces the rate of rise of the rod photoresponse by interfering with transducin expression (45,58). Phosducin levels are high in transducin α-subunit knockout mice (59), possibly in an unsuccessful attempt to restore transducin levels. Levels of phosducin were depressed in Bouse (Fig. 1) and heightened in R+/− rods that contain half the normal complement of rhodopsin (7), suggesting that regulatory control over phosducin expression is inversely linked to rod opsin expression. The normal levels of transducin α- and β-subunits in Bouse, as well as in R+/− rods, may have resulted from the changes in phosducin level. Alternatively, the changes in phosducin level may have been too small to affect transducin expression noticeably.

Instead, the reduction in amplification was attributed to structural alterations of the outer segment. An amplification factor for phototransduction was defined as (42)

$$A = \nu_{RE}(0.5k_{cat}/K_m)(n_{cGMP})/(NVB), \quad (5)$$

where k_{cat}/K_m characterizes the hydrolytic prowess of a PDE catalytic subunit, N is Avogadro's number, V is the aqueous cytosolic volume of the outer segment, B is a cGMP buffering constant, and n_{cGMP} is the Hill coefficient of the CNG channel for cGMP. The enlarged outer-segment diameter had two consequences relevant to the onset of the flash response. First, transducin and other membrane proteins expressed at normal levels were dispersed over a 1.6-fold greater disk membrane surface area, causing ν_{RE} to decline. Second, with a 1.1-fold increase in intradisk volume, the normal, vigorous PDE activity had to hydrolyze a greater number of cGMP molecules and therefore required more time to decrease cGMP to a given concentration (44). In both cases, the factors represent lower limits because tilting of disk membranes was not taken into account. According to Eq. 5, the net effect should be a $(1.6)(1.1) = 1.8$-fold reduction of amplification in Bouse. Our estimate of a 1.6-fold reduction in amplification in Bouse approached that expectation (Fig. 8). Although minimization of incisures in Bouse should have reduced amplification in the single-photon response by restricting the longitudinal spread of cGMP along the outer segment (60), this effect was not a consideration for saturating flash responses, because intracellular cGMP changed globally with little longitudinal variation.

This interpretation that amplification was reduced was further supported by a mathematical model that incorporated the altered biochemistry, diffusion, and geometric aspects in Bouse. However, according to the model, the normalized fractional single-photon response for Bouse should have been reduced in size, compared to that for WT. The apparent discrepancy between the recorded and simulated Bouse response amplitudes, which was not resolved by varying the numbers of channels or guanylyl cyclases, suggests that some step or steps in the shutoff and recovery process were changed.

Full recovery from the photoresponse requires the shutoff of photoexcited rhodopsin and activated transducins (9). Both shutoff processes involve collisional interactions of mobile, membrane proteins: rhodopsin with GRK1 and the transducin/PDE complex with RGS9. Scattering of normal amounts of GRK1 and RGS9 over a larger disk surface area in Bouse rods would reduce the collision rates. As shutoff of rhodopsin is a nondominant step in the photoresponse recovery, slowing it down boosts the single-photon response and extends the saturation time after bright flashes (61). Extra recoverin in Bouse rods could also have contributed to slower rhodopsin turnoff. However, the increase in recoverin level as determined by Western blot analysis was not significant and other physiologic evidence was lacking. Recoverin buffers Ca^{2+} within the outer segment, and, therefore, knockout of recoverin accelerates Ca^{2+} extrusion (49), but there were no discernable changes in the rate or in the fractional amplitude of Na^{+}/Ca^{2+}, K^{+} exchange in Bouse rods (Table 1). Recoverin modulates light-dependent PDE activity by conferring Ca^{2+}-dependent restraint to rhodopsin kinase activity (49,62,63), and so an increased level would prolong saturation time and slow dim flash-response recovery kinetics. Prolongation was not observed in Bouse (Figs. 5 and 6). Transgene-driven overexpression of RGS9 also accelerated photoresponse recovery (43) and RGS9 knockout slowed it down (64), but, except for a slightly rounded peak in the dim flash response of Bouse rods (Fig. 6), any slowing of photoresponse recovery was too small to resolve in our sample of rods. In this regard, it is notable that the Bouse transgene encodes for an extra threonine, A335T, on the carboxy terminus of rhodopsin (16) that is not normally present on mouse opsin and introduces a potential phosphorylation site. Stepwise removal of phosphorylation sites on rhodopsin's carboxy terminus slows the shutoff (65), and, therefore, increasing the number of phosphorylation sites from six to seven might have accelerated rhodopsin shutoff and partially masked an otherwise slowed recovery.

In conclusion, expression of greater-than-normal amounts of rhodopsin in rods improved photon capture but did not increase the packing density of proteins in the membrane, because rods simply enlarged their disks to accommodate the extra protein load. The enlarged disk size delayed and diminished the amplification of the photoresponse by spreading transducin and PDE over a wider surface area and by increasing the interdiskal cytosolic volume that contained cGMP. The increase in disk size also left the rod prone to outer-segment disorganization and a premature demise. It would appear that greater opsin production stimulated the formation of bigger disks, but, without a concomitant increase in rds/peripherin and other structural proteins, the larger outer segments suffered from structural instability.

We thank M. Soloviev, K. Rwayitare, and Z. Wang for technical assistance and A. M. Dizhoor, R. W. Lee, T. Li, R. S. Molday, T. G. Wensel for their generous gifts of antibodies. We also thank M. C. Cornwall for access to his microspectrophotometer for preliminary measurements, the late G. Jones for advice on its use, and P. Bisegna and G. Caruso for developing the MATLAB (The MathWorks, Natick, MA) code on which the simulations were based.

This research was supported by the Lions of Massachusetts for the Massachusetts Eye and Ear Infirmary and for the Tufts University School of Medicine; a Research to Prevent Blindness Challenge Grant to the New England Eye Center at Tufts University School of Medicine; the National Center for Research Resources; the Presbyterian Health Foundation; Research to Prevent Blindness; the Foundation Fighting Blindness, Inc.; the National Institutes of Health (GM068953); and the National Eye Institute (EY011358, EY014104, EY12008, EY04149, EY00871, EY12190, EY14052, EY11500 and EY006062).

REFERENCES

1. Jacoby, E., R. Bouhelal, M. Gerspacher, and K. Seuwen. 2006. The 7TM G-protein-coupled receptor target family. *ChemMedChem.* 1:760–782.
2. Schöneberg, T., M. Hofreiter, A. Schulz, and H. Römpler. 2007. Learning from the past: evolution of GPCR functions. *Trends Pharmacol. Sci.* 28:117–121.
3. Receptor Database, The International Union of Basic and Clinical Pharmacology (IUPHAR) accessed on http://www.iuphar-db.org.
4. Penn, J. S., and R. E. Anderson. 1992. Effects of light history on the rat retina. *Prog. Retinal Res.* 11:75–98.
5. Penn, J. S. 1998. Early studies of the photostasis phenomenon. Retinal adaptation to the light environment. *In* Photostasis and Related Phenomena. T. P. Williams and A. B. Thistle, editors. Plenum Press, New York and London, pp. 1–16.
6. Humphries, M. M., D. Rancourt, G. J. Farrar, P. Kenna, M. Hazel, et al. 1997. Retinopathy induced in mice by targeted disruption of the rhodopsin gene. *Nat. Genet.* 15:216–219.
7. Lem, J., N. V. Krasnoperova, P. D. Calvert, B. Kosaras, D. A. Cameron, et al. 1999. Morphological, physiological, and biochemical changes in rhodopsin knockout mice. *Proc. Natl. Acad. Sci. USA.* 96:736–741.
8. Pugh, E. N., Jr., and T. D. Lamb. 2000. Phototransduction in vertebrate rods and cones: molecular mechanisms of amplification, recovery and light adaptation. *In* Handbook of Biological Physics, Vol. 3: Molecular Mechanisms in Visual Transduction. D. G. Stavenga, W. J. DeGrip, and E. N. Pugh, Jr., editors. Elsevier Science, New York, pp. 183–255.
9. Fu, Y., and K. -W. Yau. 2007. Phototransduction in mouse rods and cones. *Pflugers Arch. Eur. J. Physiol.* 454:805–819.
10. Saxton, M. J., and J. C. Owicki. 1989. Concentration effects on reactions in membranes: rhodopsin and transducin. *Biochim. Biophys. Acta.* 979:27–34.
11. Fotiadis, D., Y. Liang, S. Filipek, D. A. Saperstein, A. Engel, et al. 2003. Atomic-force microscopy: Rhodopsin dimers in native disc membranes. *Nature.* 421:127–128.
12. Botelho, A. V., T. Huber, T. P. Sakmar, and M. F. Brown. 2006. Curvature and hydrophobic forces drive oligomerization and modulate activity of rhodopsin in membranes. *Biophys. J.* 91:4464–4477.
13. Dell'Orco, D., and H. Schmidt. 2008. Mesoscopic Monte Carlo simulations of stochastic encounters between photoactivated rhodopsin and transducin in disc membranes. *J. Phys. Chem. B.* 112:4419–4426.
14. Calvert, P. D., V. I. Govardovskii, N. Krasnoperova, R. E. Anderson, J. Lem, et al. 2001. Membrane protein diffusion sets the speed of rod phototransduction. *Nature.* 411:90–94.
15. Liang, Y., D. Fotiadis, T. Maeda, A. Maeda, A. Modzelewska, et al. 2004. Rhodopsin signaling and organization in heterozygote rhodopsin knockout mice. *J. Biol. Chem.* 279:48189–48196.

16. Tan, E., Q. Wang, A. B. Quiambao, X. Xu, N. M. Qtaishat, et al. 2001. The relationship between opsin overexpression and photoreceptor degeneration. *Invest. Ophthalmol. Vis. Sci.* 42:589–600.

17. Sieving, P. A., M. L. Fowler, R. A. Bush, S. Machida, P. D. Calvert, et al. 2001. Constitutive ''light'' adaptation in rods from G90D rhodopsin: a mechanism for human congenital nightblindness without rod cell loss. *J. Neurosci.* 21:5449–5460.

18. Lee, R. H., J. P. Whelan, R. N. Lolley, and J. F. McGinnis. 1988. The photoreceptor-specific 33 kDa phosphoprotein of mammalian retina: generation of monospecific antibodies and localization by immunocytochemistry. *Exp. Eye Res.* 46:829–840.

19. Dizhoor, A. M., S. Ray, S. Kumar, G. Niemi, M. Spencer, et al. 1991. Recoverin: a calcium sensitive activator of retinal rod guanylate cyclase. *Science.* 251:915–918.

20. Yang, J., X. Liu, G. Yue, M. Adamian, O. Bulgakov, et al. 2002. Rootletin, a novel coiled-coil protein, is a structural component of the ciliary rootlet. *J. Cell Biol.* 159:431–440.

21. Liu, X., O. V. Bulgakov, X. -H. Wen, M. L. Woodruff, B. Pawlyk, et al. 2004. AIPL1, the protein that is defective in Leber congenital amaurosis, is essential for the biosynthesis of retinal rod cGMP phosphodiesterase. *Proc. Natl. Acad. Sci. USA.* 101:13903–13908.

22. Illing, M., L. L. Molday, and R. S. Molday. 1997. The 220-kDa rim protein of retinal rod outer segments is a member of the ABC transporter superfamily. *J. Biol. Chem.* 272:10303–10310.

23. Makino, C. L., X. -H. Wen, N. Michaud, I. V. Peshenko, B. Pawlyk, et al. 2006. Effects of low AIPL1 expression on phototransduction in rods. *Invest. Ophthalmol. Vis. Sci.* 47:2185–2194.

24. Mazia, D., G. Schatten, and W. Sale. 1975. Adhesion of cells to surfaces coated with polylysine. *J. Cell Biol.* 66:198–200.

25. Brockerhoff, S. E., J. B. Hurley, U. Janssen-Bienhold, S. C. Neuhauss, W. Driever, et al. 1995. A behavioral screen for isolating zebrafish mutants with visual system defects. *Proc. Natl. Acad. Sci. USA.* 92:10545–10549.

26. Makino, C. L., L. N. Howard, and T. P. Williams. 1990. Axial gradients of rhodopsin in light-exposed retinal rods of the toad. *J. Gen. Physiol.* 96:1199–1220.

27. Makino, C. L., X. -H. Wen, and J. Lem. 2003. Piecing together the timetable for visual transduction with transgenic animals. *Curr. Opin. Neurobiol.* 13:404–412.

28. Wacker, W. B., L. A. Donoso, C. M. Kalsow, J. A. Yankeelov, Jr., and D. T. Organisciak. 1977. Experimental allergic uveitis. Isolation, characterization, and localization of a soluble uveitopathogenic antigen from bovine retina. *J. Immunol.* 119:1949–1958.

29. Yajima, S., F. Seki, S. Takano, and M. Usui. 1983. Localization of S-antigen by enzyme-labeled antibody method and electron microscopy. *Jpn. J. Ophthalmol.* 27:526–534.

30. Van der Spuy, J., J. P. Chapple, B. J. Clark, P. J. Luthert, C. S. Sethi, et al. 2002. The Leber congenital amaurosis gene product AIPL1 is localized exclusively in rod photoreceptors of the adult human retina. *Hum. Mol. Genet.* 11:823–831.

31. Papermaster, D. S., C. A. Converse, and M. Zorn. 1976. Biosynthetic and immunochemical characterization of a large protein in frog and cattle rod outer segment membranes. *Exp. Eye Res.* 23:105–115.

32. Molday, R. S., D. Hicks, and L. Molday. 1987. Peripherin. A rim-specific membrane protein of rod outer segment discs. *Invest. Ophthalmol. Vis. Sci.* 28:50–61.

33. Anderson, R. E., M. B. Maude, and D. Bok. 2001. Low docosahexaenoic acid levels in rod outer segment membranes of mice with *rds*/peripherin and P216L peripherin mutations. *Invest. Ophthalmol. Vis. Sci.* 42:1715–1720.

34. Carter-Dawson, L. D., and M. M. LaVail. 1979. Rods and cones in the mouse retina. I. Structural analysis using light and electron microscopy. *J. Comp. Neurol.* 188:245–262.

35. Nickell, S., P. S. -H. Park, W. Baumeister, and K. Palczewski. 2007. Three-dimensional architecture of murine rod outer segments determined by cryoelectron tomography. *J. Cell Biol.* 177:917–925.

36. Cohen, A. I. 1960. The ultrastructure of the rods of the mouse retina. *Am. J. Anat.* 107:23–48.

37. Govardovskii, V. I., N. Fyhrquist, T. Reuter, D. G. Kuzmin, and K. Donner. 2000. In search of the visual pigment template. *Vis. Neurosci.* 17:509–528.

38. Hestrin, S., and J. I. Korenbrot. 1990. Activation kinetics of retinal cones and rods: response to intense flashes of light. *J. Neurosci.* 10:1967–1973.

39. Baylor, D. A., T. D. Lamb, and K. -W. Yau. 1979. Responses of retinal rods to single photons. *J. Physiol.* 288:613–634.

40. Bisegna, P., G. Caruso, D. Andreucci, L. Shen, V. V. Gurevich, et al. 2008. *Biophys. J.* 94:3363–3383.

41. Pepperberg, D. R., M. C. Cornwall, M. Kahlert, K. P. Hofmann, J. Jin, et al. 1992. Light-dependent delay in the falling phase of the retinal rod photoresponse. *Vis. Neurosci.* 8:9–18.

42. Lyubarsky, A., S. Nikonov, and E. N. Pugh, Jr. 1996. The kinetics of inactivation of the rod phototransduction cascade with constant Ca^{2+}_i. *J. Gen. Physiol.* 107:19–34.

43. Krispel, C. M., D. Chen, N. Melling, Y. -J. Chen, K. A. Martemyanov, et al. 2006. RGS expression rate-limits recovery of rod photoresponses. *Neuron.* 51:409–416.

44. Lamb, T. D., and E. N. Pugh, Jr. 1992. A quantitative account of the activation steps involved in phototransduction in amphibian photoreceptors. *J. Physiol.* 449:719–758.

45. Krispel, C. M., M. Sokolov, Y. -M. Chen, H. Song, R. Herrmann, et al. 2007. Phosducin regulates the expression of transducin $\beta\gamma$ subunits in rod photoreceptors and does not contribute to phototransduction adaptation. *J. Gen. Physiol.* 130:303–312.

46. Yau, K. -W., and K. Nakatani. 1984. Electrogenic Na-Ca exchange in retinal rod outer segment. *Nature.* 311:661–663.

47. Cervetto, L., L. Lagnado, R. J. Perry, D. W. Robinson, and P. A. McNaughton. 1989. Extrusion of calcium from rod outer segments is driven by both sodium and potassium gradients. *Nature.* 337:740–743.

48. Burns, M. E., A. Mendez, J. Chen, and D. A. Baylor. 2002. Dynamics of cyclic GMP synthesis in retinal rods. *Neuron.* 36:81–91.

49. Makino, C. L., R. L. Dodd, J. Chen, M. E. Burns, A. Roca, et al. 2004. Recoverin regulates light-dependent phosphodiesterase activity in retinal rods. *J. Gen. Physiol.* 123:729–741.

50. Marszalek, J. R., X. Liu, E. A. Roberts, D. Chui, J. D. Marth, et al. 2000. Genetic evidence for selective transport of opsin and arrestin by kinesin-II in mammalian photoreceptors. *Cell.* 102:175–187.

51. Bhowmick, R., and J.C. Besharse. 2007. Identification of a chaperone mediated cargo complex association with intraflagellar transport proteins in photoreceptor. 2007 ARVO Annual Meeting Abstracts. *Invest. Ophthalmol. Vis. Sci.* 48:3799. (Abstr.)

52. Partridge, J. C., S. N. Archer, and J. N. Lythgoe. 1988. Visual pigments in the individual rods of deep-sea fishes. *J. Comp. Physiol. [A].* 162:543–550.

53. Partridge, J. C., J. Shand, S. N. Archer, J. N. Lythgoe, and W. A. H. M. van Groningen-Luyben. 1989. Interspecific variation in the visual pigments of deep-sea fishes. *J. Comp. Physiol. [A].* 164:513–529.

54. Clarke, G., A. F. X. Goldberg, D. Vidgen, L. Collins, L. Ploder, et al. 2000. Rom-1 is required for rod photoreceptor viability and the regulation of disk morphogenesis. *Nat. Genet.* 25:67–73.

55. Goldberg, A. F. X. 2006. Role of peripherin/rds in vertebrate photoreceptor architecture and inherited retinal degenerations. *Int. Rev. Cytol.* 253:131–175.

56. Pazour, G. J., S. A. Baker, J. A. Deane, D. G. Cole, B. L. Dickert, et al. 2002. The intraflagellar transport protein, IFT88, is essential for vertebrate photoreceptor assembly and maintenance. *J. Cell Biol.* 157:103–114.

57. Travis, G. H., K. R. Groshan, M. Lloyd, and D. Bok. 1992. Complete rescue of photoreceptor dysplasia and degeneration in transgenic retinal degeneration slow (rds) mice. *Neuron.* 9:113–119.

58. Sokolov, M., K. J. Strissel, I. B. Leskov, N. A. Michaud, V. I. Govardovskii, et al. 2004. Phosducin facilitates light-driven transducin

translocation in rod photoreceptors. Evidence from the phosducin knockout mouse. *J. Biol. Chem.* 279:19149–19156.

59. Calvert, P. D., N. V. Krasnoperova, A. L. Lyubarsky, T. Isayama, M. Nicoló, et al. 2000. Phototransduction in transgenic mice after targeted deletion of the rod transducin α-subunit. *Proc. Natl. Acad. Sci. USA.* 97:13913–13918.
60. Caruso, G., P. Bisegna, L. Shen, D. Andreucci, H. E. Hamm, and E. DiBenedetto. 2006. Modeling the role of incisures in vertebrate phototransduction. *Biophys. J.* 91:1192–1212.
61. Sagoo, M. S., and L. Lagnado. 1997. G-protein deactivation is rate-limiting for shut-off of the phototransduction cascade. *Nature.* 389:392–395.
62. Hurley, J. B., and J. Chen. 2001. Evaluation of the contributions of recoverin and GCAPs to rod photoreceptor light adaptation and recovery to the dark state. *Prog. Brain Res.* 131:395–405.
63. Sampath, A. P., K. J. Strissel, R. Elias, V. Y. Arshavsky, J. F. McGinnis, et al. 2005. Recoverin improves rod-mediated vision by enhancing signal transmission in the mouse retina. *Neuron.* 46:413–420.
64. Chen, C. -K., M. E. Burns, W. He, T. G. Wensel, D. A. Baylor, et al. 2000. Slowed recovery of rod photoresponse in mice lacking the GTPase accelerating protein RGS9–1. *Nature.* 403:557–560.
65. Mendez, A., M. E. Burns, A. Roca, J. Lem, L. -W. Wu, et al. 2000. Rapid and reproducible deactivation of rhodopsin requires multiple phosphorylation sites. *Neuron.* 28:153–164.